JASA EXPRESS LETTERS

https://doi.org/10.1121/10.0001333

Passive geoacoustic inversion in the Mid-Atlantic Bight in the presence of strong water column variability

Tsu Wei Tan,[1,a)] Oleg A. Godin,[1,b)] Boris G. Katsnelson,[2,c)] and Marina Yarina[2]

[1]*Physics Department, Naval Postgraduate School, Monterey, California 93943, USA*

[2]*Department of Marine Geosciences, University of Haifa, Haifa, Israel*

ttan1@nps.edu, oagodin@nps.edu, bkatsnels@univ.haifa.ac.il, yarina_marina@icloud.com

Abstract: Empirical Green's functions are obtained for 31 paths in a highly dynamic coastal ocean by cross-correlation of ambient and shipping noise recorded in the Shallow Water 2006 experiment on a horizontal line array and a single hydrophone about 3600 m from the array. Using time warping, group speeds of three low-order normal modes are passively measured in the 10–110 Hz frequency band and inverted for geoacoustic parameters of the seabed. It is demonstrated that, despite very strong sound speed variations caused by nonlinear internal waves, noise interferometry can be successfully used to acoustically characterize the seafloor on a continental shelf.

[Editor: Charles C. Church] Pages: EL453–EL459

Received: 28 March 2020 **Accepted:** 13 May 2020 **Published Online:** 2 June 2020

1. Introduction

Acoustic noise interferometry[1–3] exploits ambient and shipping noise as a signal to probe the ocean and offers a way to measure its physical parameters without using any controlled sound sources.[4–9] The technique relies on time averaging to retrieve an approximation to the deterministic Green's function (GF), or empirical GF, from noise cross-correlations. In shallow water, the basic assumption[1,3,10] that the environment does not change during noise averaging time is hardly compatible with temporal variability of the ocean. Theory[11] and experiments in coastal oceans with mild temporal variability[5,8] indicate that this assumption can be significantly relaxed. The goal of this paper is to investigate the feasibility of using noise interferometry for passive acoustic characterization of the seabed in a coastal ocean with strong and rapid variations of the water column properties. We obtain empirical GFs from noise cross-correlation functions (NCCFs) on multiple paths in a highly dynamic environment[12,13] on a continental shelf in the Mid-Atlantic Bight (Sec. 2), apply time-warping transform[14–17] to retrieve dispersion curves of normal modes from the GFs (Sec. 3), invert the passively measured dispersion curves to estimate parameters of the seabed (Sec. 4), and analyze the results of the passive geoacoustic inversion (Sec. 5).[18] From retrieving empirical GFs to inversions, we largely follow the approach recently applied[16] to another dataset that was obtained in a much more stable environment.

2. Experimental data and noise cross-correlations

The data employed in this study are the records of shipping and ambient noise obtained in the course of the Shallow Water 2006 (SW06) experiment[12,13] in the Mid-Atlantic Bight off New Jersey. We use time series of noise continuously recorded during 15 days from August 18 to September 1, 2006 on a Single Hydrophone Receiving Unit (SHRU) and 32-hydrophone horizontal line array (HLA). The spacing of HLA hydrophones is 15 m, and the distance between SHRU and the HLA hydrophones ranges between 3.4 and 3.8 km [Fig. 1(a)]. SHRU and HLA hydrophones are located close to the seafloor. The two systems share the same sampling frequency and data format,[12] which facilitates data processing.

The SW06 site is known for strong and rapid variations of the sound speed in the water column due to energetic internal gravity waves, including internal tides.[13] Figure 1(b) shows sound speed measured with a vertical thermistor chain[12] that was deployed in the vicinity of the southern end of the HLA. Internal tides depress the thermocline by tens of meters in a

[a)]Author to whom correspondence should be addressed. Also at: Department of Marine Science, ROC Naval Academy, Taiwan, ORCID: 0000-0002-1145-9349.

[b)]ORCID: 0000-0003-4599-2149.

[c)]ORCID: 0000-0001-8934-5504.

https://doi.org/10.1121/10.0001333

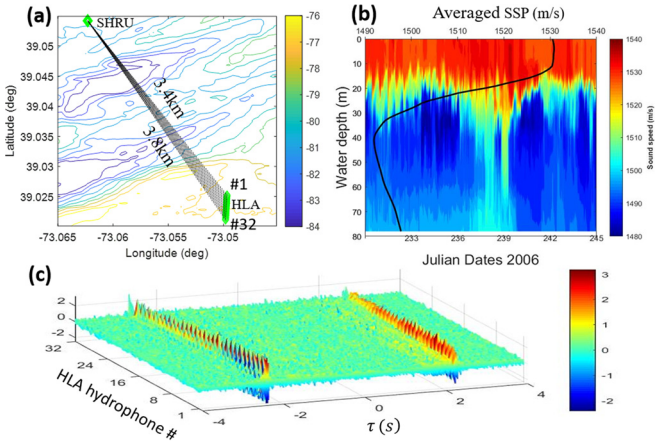

Fig. 1. (Color online) Bathymetry, sound speed, and two-point cross-correlation functions of noise measured during the SW06 experiment. (a) Locations of the SHRU and HLA employed in this study. Water depth in meters is shown by isobaths. (b) Time-dependence of the sound speed in water measured at a location near the northern end of the HLA, with the 15-day average of the SSP (black line) superimposed. (c) NCCFs in arbitrary units between SHRU and individual hydrophones of HLA are shown as functions of the time delay τ and the number, 1 to 32, of the HLA hydrophone. NCCFs are calculated using 15 days of noise records.

quasi-periodic manner causing sound speed variations up to 13 m/s from the mean [Fig. 1(b)] and making the environment rather challenging for application of acoustic noise interferometry.

We have calculated cross-correlation functions between the acoustic pressure recorded at SHRU and each of the HLA hydrophones [Fig. 1(c)]. Following Refs. 5 and 16, NCCFs between SHRU and the ith hydrophone of HLA is first evaluated in the frequency domain as an average over N non-overlapping time windows,

$$\hat{C}_i(f) = \frac{1}{N}\sum_{n=1}^{N} \frac{P_S^{(n)}(f) P_{H,i}^{(n)}(f)^*}{|P_S^{(n)}(f) P_{H,i}^{(n)}(f)^*|}, \quad i = 1, 2, \ldots, 32. \tag{1}$$

Here the asterisk * denotes complex conjugation; $P_S^{(n)}(f)$ and $P_{H,i}^{(n)}(f)$ are the spectra of pressure recorded during the nth time window by SHRU and ith HLA hydrophone, respectively. Normalizing the spectra by their absolute values in the summand in Eq. (1) implements the spectral pre-whitening that, in the noise interferometry context, is known to suppress contributions of strong, transient non-diffuse noise sources such as nearby shipping.[4,5] The time domain NCCFs $C_i(\tau)$ are obtained via inverse Fourier transform of Eq. (1). For brevity, the negative ($\tau < 0$) and positive ($\tau > 0$) time-delay parts of $C_i(\tau)$ will be referred to as N-NCCF and P-NCCF. These approximate, respectively, the acoustic GFs that describe sound propagation from the ith HLA hydrophone to SHRU and from SHRU to the hydrophone.[1,3]

A time-window length of 64 s was chosen in implementing Eq. (1). HLA hydrophone #31 malfunctioned during the experiment[27] and did not produce useable data. Thus, NCCFs were obtained only for 31 receiver pairs. In motionless media with perfectly diffuse noise, NCCFs are even functions of τ,[1,3] and asymmetry of measured NCCFs is due to a shift between the internal clocks used at the two receivers.[5,8] Cross-correlation of the P-NCCF with the N-NCCF for the same receiver pair, which was done for all 31 pairs, revealed a shift of 0.896 s between the SHRU and HLA clocks. Being much smaller than the time-window length, the clock shift has a negligible effect on the quality of NCCF estimates and has been corrected for by shifting all $C_i(\tau)$ by 0.896 s along the time-delay axis.

With random noise sources, the sum in the right side of Eq. (1) is also a random function. In a time-independent environment, it is expected to converge to a deterministic NCCF when noise averaging time is sufficiently long,[4,10] i.e., the number N of time windows is sufficiently large. Animation Mm. 1 shows the evolution of the time-domain NCCF estimate based on Eq. (1) for 31 receiver pairs, when noise averaging time increases from 1 to 15 days, starting from August 18, 2006. The frequency band 10 Hz $< f <$ 110 Hz is used to obtain the time-domain NCCFs in Fig. 1(c) and animations Mm. 1 and Mm. 2. The deterministic features of the NCCFs gradually emerge and become increasingly clear as more daily averages are stacked, as shown in Mm. 1. About 10 days of noise averaging is sufficient to reach a stable estimate of all NCCFs. Since noise sources are intermittent, the signal strengths of both P-NCCFs and N-NCCFs do not increase monotonically. [In noise interferometry, the deterministic component of NCCF estimates serves as the signal, and the signal-to-noise ratio (SNR) is understood to be the ratio of

https://doi.org/10.1121/10.0001333

amplitudes of the deterministic and random components of an NCCF estimate.] It is interesting to observe that P-NCCFs accumulate faster than N-NCCFs in the first 5 days, and after that both approach stability in a qualitatively similar way. We found that certain days, such as days 6 and 12 in Mm. 1, produce N-NCCF estimates with a particularly high SNR. Averaging noise recorded during 2–3 of such "good days" results in N-NCCF estimates with a SNR close to that of the much longer, 15-day averages shown in Fig. 1(c).

Mm. 1. Cumulative 15-day averages of NCCFs from August 18–September 1. This is a file of type "gif" (1139 kb).

Mm. 2. Waveforms of 15-day averaged 31 P-NCCFs and N-NCCFs. This is a file of type "gif" (796 kb).

Animation Mm. 2 shows individual P-NCCFs and N-NCCFs of $C_i(\tau)$ in Fig. 1(c) in the order of increasing $i = 1, 2, \ldots, 32$. Note that SNR decreases as the horizontal distance from SHRU to the HLA hydrophone increases. The decrease appears to be faster than that of the GF amplitude. This can be due, in part, to the noise directivity in the horizontal plane.[3] Variations of the sound speed profile (SSP) and sea surface geometry in time also contribute to the more rapid decrease of the NCCF's SNR with range than in the time-independent environment.[11] Moreover, the suppression of the coherent (deterministic) component of NCCF estimates due to time dependence of the propagation conditions tends to increase with acoustic frequency.[11] For individual normal mode components of NCCF in a shallow-water waveguide, the suppression is also predicted to increase with the mode order.[11] We found that SNR of the Eq. (1)-based NCCF estimate becomes rather low and the signal is lost in noise at frequencies above about 110 Hz. No useful NCCFs were derived from the available data at these frequencies. We attribute this to the coherence loss of time averages in the rapidly evolving environment. The subsequent analysis will be limited to the 10–110 Hz frequency band.

Animations Mm. 1 and Mm. 2 show additional NCCF peaks that appear at positive time delays τ shortly before the main peaks of P-NCCFs. The additional peaks form a line in Fig. 1(c). We interpret the additional peak as a spurious arrival from a non-diffuse noise source. The position of the additional peaks is found to be consistent with the non-diffuse noise source being the shipping lanes leading to and from New York Harbor, which is located about 120 nm from the HLA. The same interpretation was proposed earlier[19] for the spurious arrival observed in the NCCF for a different pair of SW06 receivers. The spurious arrivals partially overlap with the main peaks and distort the P-NCCFs, especially on the northern side of HLA [Fig. 1(a)]. Because of this, only N-NCCFs are used in this study as the input data to retrieve normal mode dispersion curves and perform geoacoustic inversions.

3. Retrieving acoustic normal mode travel times by time warping

Time warping transform maps a signal $S(\tau)$ into the "warped" signal

$$\tilde{S}(w(\tau)) = |dw(\tau)/d\tau|^{-1/2} S(\tau), \tag{2}$$

where $w(\tau)$ has the meaning of time in the warped domain. Transform (2) with the warping function $w(\tau) = (\tau^2 - \tau_r^2)^{1/2}$ has been used successfully to isolate normal mode components of acoustic field in shallow-water waveguides.[14–16] Here $\tau = 0$ at the moment when the signal is emitted by a sound source. Reference time τ_r in the warping function can be defined as $\tau_r = r/c_w$, where r is the sound propagation range and c_w is a representative value of sound speed in water. In the noise interferometry context, and r is the distance between two receivers. The inverse time-warping transform, which restores the original signal from the warped one, is again given by Eq. (2) but with $w(\tau) = (\tau^2 + \tau_r^2)^{1/2}$.[14]

We use measured N-NCCFs as the signals interrogating the environment. Then $S_i(\tau) = C_i(-\tau)$, $\tau > 0$, $i = 1, 2, \ldots, 32$. The spectrogram of $S_1(\tau)$ is shown in Fig. 2(a). The spectrogram shows strong mode interference that manifests itself most clearly in a sequence of deep interference nulls. It does not appear possible to identify individual mode contributions, let alone retrieve mode dispersion curves from the spectrogram. However, normal mode components occupy distinct frequency bands and are clearly separated in the spectrogram of the warped signal $\tilde{S}_1(w)$ in Fig. 2(b). In the warping function $w(\tau)$, τ_r has the meaning of the earliest arrival time of the received signal being warped. For each receiver pair, it has been determined from the condition that modes are best separated and fully resolved in the warped domain. For instance, the optimum reference time for $\tilde{S}_1(w)$ is $\tau_r \approx 2.28$ s. Equivalent values of c_w in the equation $\tau_r = r/c_w$ for the optimum reference times prove to be close to the minimum of the SSP in Fig. 1(b).

The spectrogram of the warped signal allows one to define time-frequency (TF) masks[14] as areas in the warped time-warped frequency plane, where energy of a single mode is concentrated and no other modes are present. The TF mask of a particular mode is illustrated in Fig. 2(b). To isolate the contribution of mode m to the signal $S_i(\tau)$, the respective TF mask is applied

JASA EXPRESS LETTERS

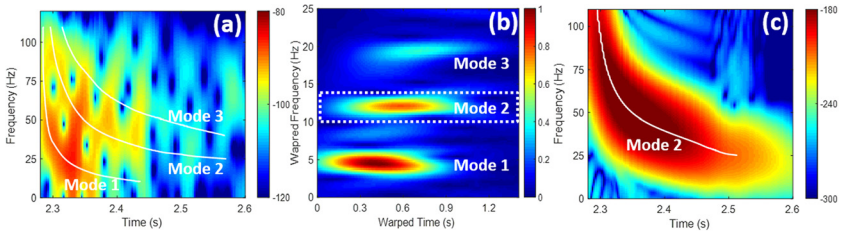

Fig. 2. (Color online) Application of the time-warping transform to a measured NCCF to separate its normal-modal components and passively measure dispersion curves of the normal modes. (a) Spectrogram of the negative-time-delay part, N-NCCF, of the cross-correlation $C_1(\tau)$ between SHRU and the first HLA hydrophone. Spectral density is shown in dB relative to an arbitrary reference. Overlaid white lines display estimated dispersion curves of the first three normal modes. (b) Spectrogram of the same N-NCCF after time warping. Contributions of individual normal modes are indicated. The area within the white dashed lines is the TF mask applied to isolate mode 2 as an unwarping stage of signal processing. (c) Spectrogram of the mode 2 waveform after unwarping. White line shows the mode 2 dispersion curve retrieved from the spectrogram.

to the short-time Fourier transform of $\mathring{S}_i(w)$. The inverse short-time Fourier transform of the result gives the mode's waveform in the warped domain, which is unwarped back to the physical domain by application of the inverse time-warping transform. A spectrogram of the mode 2 component of $S_1(\tau)$ is illustrated in Fig. 2(c). As expected, it shows no signs of mode interference.

In a spectrogram of a single-mode, broadband waveform the peak values with respect to time at any given frequency lie close to the travel time, which corresponds to the mode's group speed at that frequency. Dependence of the travel time on frequency is most accurately extracted from the spectrogram using the reassignment process,[20] which improves the resolution of TF distribution by reallocating the energy concentration. The result of application of the reassignment process is illustrated in Fig. 2(c) for mode 2 component of signal $S_1(\tau)$. This procedure was repeated and frequency dependence of the travel time was determined for the first three modes using optimum, mode-, and HLA hydrophone-specific TF masks for all 31 measured N-NCCFs.

4. Geoacoustic inversion

The input acoustic data for a geoacoustic inversion (Fig. 3) are the travel times of modes $m = 1$–3 measured on 31 paths. Assuming range-independent propagation, for each mode m the data can be combined in terms of the group speed $g_{i,m}(f) = r_i/t_{i,m}(f)$ of the mode. Here r_i and $t_{i,m}$ are the horizontal distance[12] and measured travel time between SHRU and the ith HLA hydrophone. Averaging $g_{i,m}$ over i has the advantage of significantly suppressing random measurement errors. The frequency dependence of the path-averaged group speeds $\bar{g}_m(f)$ and uncertainty of their measurements are illustrated in Fig. 3(b). The uncertainty is evaluated at each frequency as the square root of the sample variance of 31 measurements.

The actual propagation environment is horizontally inhomogeneous. The water depths at SHRU and HLA are 82 and 78 m, respectively.[12] Within the triangle with vertices at SHRU and hydrophones 1 and 32 of HLA [Fig. 1(a)], water depths are 76–85 m with the average of 80.6 m. We modeled the effect of bathymetry on the mode travel times in the $N \times 2$D approximation assuming adiabatic propagation.[21] Water column and seabed parameters in the simulations were taken from the optimal environmental model [see Fig. 3(a) and Table 1] discussed later in this section. We found that the differences between travel times over actual, range-dependent bathymetry on a path and in the range-independent waveguide with the path-average water depth to be small compared to the measurement errors on a single path. For instance, for $m = 2$ and on a typical path $i = 16$ at a frequency of 50 Hz, range dependence of the bathymetry changes the mode travel time by about 30% of the measurement uncertainty shown in Fig. 3(b). The largest effects of the range-dependence were found for mode 3, for which measurement uncertainties are also larger. In the simulations, effects of changes in the path-averaged depth were found to be significantly stronger than those of variations from the average. Similarly, we found the effects of range dependence of the sound speed in the water column on the mode travel times to be small compared to the measurement uncertainty.[18] We conclude that, with the data available, the advantages of measurement error suppression by path averaging far outweigh any possible benefits of including a range-dependent bathymetry or sound speed in geoacoustic inversions.

We conduct a geoacoustic inversion assuming a range-independent environmental model with a fluid seabed formed by a homogeneous sediment layer overlying a homogeneous half-space, and a known SSP in water [Fig. 3(a)]. Sound speed in the water column is given by the time-averaged profile shown in Fig. 1(b). The unknown parameters of the model are the water depth D, sediment layer thickness H, sound speeds c_s, c_b in the sediment and basement, the ratios

JASA EXPRESS LETTERS
https://doi.org/10.1121/10.0001333

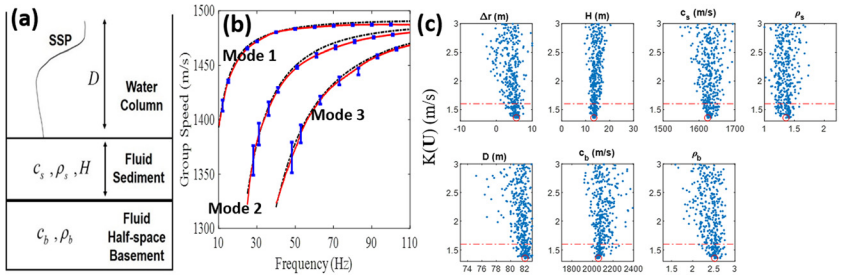

Fig. 3. (Color online) Geoacoustic inversion. (a) Range-independent environmental model implied in the inversion process. The seven unknown parameters to be determined are the water depth D, sediment layer thickness H, sound speeds c_s, c_b in the sediment and basement, and the ratios ρ_s, ρ_b of densities in the sediment and basement to that in seawater, and the correction Δr (not shown) to the nominal distance between SHRU and HLA. SSP in water is assumed to be known. (b) Normal mode dispersion curves. Solid lines are the passively measured frequency dependencies of the mode group speeds, with error bars shown for selected frequency bins. Dashed lines are the dispersion curves in the best-fitting environment found by solving the inverse problem. (c) Sensitivity of the data-model mismatch to individual parameters of the environmental model. In each panel, the cost function $K(\mathbf{U})$, Eq. (3), is plotted as a function of a single search parameter for the values of the other six parameters that were encountered during the optimization process. The circle indicates the position of the cost function minimum $K(\hat{\mathbf{U}}) = 1.35$ m/s and the inferred value of each parameter. The dashed line corresponds to the error bounds in Table 1. Only values of $K(\mathbf{U})$ up to 3 m/s are shown.

ρ_s, ρ_b of densities in the sediment and half-space to that in seawater, and the distance correction Δr. The latter is assumed to be the same for all 31 hydrophone pairs and is intended to capture the effect of deviations of the SHRU and HLA hydrophones from their nominal[12] positions.

The unknown parameters are found by minimizing the root-mean-square mismatch

$$K(\mathbf{U}) = \sqrt{\sum_{m=1}^{M} \frac{1}{M N_m} \sum_{n=1}^{N_m} [\bar{g}_m(f_n) - \hat{g}_m(f_n, \mathbf{U})]^2}, \tag{3}$$

between the measured, $\bar{g}_m(f)$, and modeled group speeds of normal modes. Here $M = 3$ is the number of normal modes identified, and N_m is the number of frequency bins to be compared between the measured and modeled dispersion curves of mode m. Non-overlapping bins of 0.2 Hz width are used in the 10–110, 25–110, and 40–110 Hz frequency bands for modes 1, 2, and 3, respectively. The modeled group speeds $\hat{g}_m(f_n, \mathbf{U})$ are calculated by the normal mode code KRAKEN (Ref. 22) for various values of the vector $\mathbf{U} = \{D, H, c_s, \rho_s, c_b, \rho_b\}$ of unknown environmental parameters [Fig. 3(a)]. The distance correction Δr re-calibrates the average $\bar{g}_m(f)$ of the measured modal group speeds in Eq. (3), which are calculated as $g_{i,m}(f) = (r_i + \Delta r)/t_{i,m}(f)$.

To find the global minimum of the cost function (3), we used a MATLAB genetic algorithm[23] with a population of 64 individuals and a crossover fraction of 0.8. The algorithm was run until improvements in $K(\mathbf{U})$ fell below 10^{-3} m/s. The procedure was repeated with 14 different initial populations, resulting in the same global minimum $K(\hat{\mathbf{U}}) \approx 1.350$ m/s. Search bounds and results are summarized in Table 1. The choice of the search bounds for the geoacoustic parameters was informed by results of the previous geoacoustic studies[14,19,24–26,30] at the SW06 site.

Figure 3(b) compares normal mode dispersion curves in the optimal environmental model, which minimizes the data-model mismatch $K(\mathbf{U})$, with the measured group speeds. Note that the mismatch is small compared to measurement uncertainties, except at higher frequencies, where modal group speeds are most sensitive to variations of the sound speed in water. The inverted value $\Delta r = 5.6$ m of the distance correction falls within the uncertainty of GPS measurements that were used to calculate the nominal positions[12] of the hydrophones. As a function of water depth D, the mismatch is minimal at $D = 82.0$ m. This value coincides with the water depth

Table 1. Geoacoustic inversion parameters and results.

Parameter	Unit	Search bounds	Step	Estimated value	Error bounds
Δr	m	[−10, 10]	0.1	5.6	[3.4, 6.6]
H	m	[1, 30]	0.1	13.4	[12.3, 14.7]
c_s	m/s	[1500, 1700]	1	1624	[1612, 1651]
ρ_s	—	[1, 2.2]	0.01	1.36	[1.21, 1.49]
D	m	[73, 83]	0.1	82.0	[81.0, 82.9]
c_b	m/s	[1700, 2400]	1	2058	[2006, 2135]
ρ_b	—	[1.3, 3.0]	0.01	2.52	[2.31, 2.72]

at the SHRU location and, as expected, is close to the average water depth, 80.6 m, along the propagation paths shown in Fig. 1(a). Other inverted environmental parameters are discussed in Sec. 5 and compared to geoacoustic models derived in other studies.

Sensitivity of the cost function $K(\mathbf{U})$ to variations of individual search parameters around the optimal environmental model is illustrated in Fig. 3(c). To estimate the uncertainty of the inversion results, we compare the increase of the cost function $K(\mathbf{U})$ from its minimal value to the measurement errors. The root-mean-square measurement error of path-averaged modal groups speeds is 0.245 m/s and is shown as a red dashed-line $K(\mathbf{U}) = 1.595$ m/s in each sub-panel of Fig. 3(c). The inversion error bounds in Table 1 are found as the shortest contiguous parameter range that contains 95% of the inversion results with $K(\mathbf{U}) \leq 1.595$ m/s.

5. Discussion

As demonstrated in Secs. 3 and 4, empirical GFs have been retrieved from NCCFs in the 10–110 Hz frequency band with accuracy sufficient to characterize geoacoustic properties of the seabed, despite very strong variations of the sound speed in water [Fig. 1(b)] during the noise averaging time. Application of noise interferometry to SW06 data was first reported at much shorter ranges from tens to a few hundred meters[27,28] and with shorter averaging times. No environmental information was retrieved from the short-range empirical GFs, which were obtained in the 20–100 Hz band.[27,28] With 5.7-day noise averaging time, Qin *et al.*[19] calculated NCCF in the 10–70 Hz band for two SHRUs about 8 km apart and used the passive time-reversal mirror technique to carry out a single-parameter geoacoustic inversion assuming a homogeneous fluid seabed. From a subset of the data employed in the present study, Tan *et al.*[29] found empirical GFs in the 10–90 Hz frequency band from 7-day noise averages and performed a time-warping-based geoacoustic inversion using a single hydrophone pair. Compared to previous work,[29] a longer averaging time and especially combining the results for 31 hydrophone pairs have allowed us here to expand the bandwidth and significantly increase the accuracy of retrieval of mode dispersion curves from the noise cross-correlations. Extensive work on geoacoustic inversions at the SW06 site was done using controlled sound sources.[30] Results of the active inversions are consistent with the results in Table 1 within their uncertainties.[18]

Within the chosen parameterization of the seabed properties [Fig. 3(a)], robustness of the passive geoacoustic inversion was investigated by employing a different cost function and varying the bandwidth of input data. If the cost function is chosen as the mismatch in the path-average of the group slowness, $1/g_{i,m}(f_n)$, rather than the mode group speed $g_{i,m}(f_n)$, solution of the inverse problem changes insignificantly: $\Delta r = 4.9$ m, $H = 13.1$ m, $c_s = 1624$ m/s, $\rho_s = 1.30$, $D = 81.1$ m, $c_b = 2058$ m/s, $\rho_b = 2.54$ with a similar size of error bounds for each inverted parameter as in Table 1.

Using mode group speed measurements at the lowest available frequencies was found critical to ensure sensitivity to the sediment layer and especially the half-space parameters. In contrast, decreasing the upper frequency from 110 to 90 Hz appreciably changed only the optimum value of the water depth, which increased to $D = 82.9$ m. Estimates of the other inverted parameters remained well within their error bounds in Table 1. This observation is consistent with results of the forward modeling, which show that the group speeds are most sensitive to sound speed in water at $f = 90$–110 Hz, and suggests the possibility of using the upper part of the available frequency band to characterize water column properties.

6. Conclusion

We have demonstrated that robust estimates of empirical GFs can be obtained from noise cross-correlations in a dynamic coastal ocean despite internal wave-induced strong, rapid variations of the water column sound speed. Passively measured dispersion curves of low-order acoustic normal modes have been inverted for geoacoustic parameters of the seabed. The results are largely consistent with earlier geoacoustic inversions employing controlled sound sources in the same general area.

Future work includes using a higher-frequency portion of passively measured modal dispersion curves to characterize the water column variability and extending geoacoustic inversions to horizontally inhomogeneous environmental models.

Acknowledgments

The data used in this study were collected by the Woods Hole Oceanographic Institution. The authors are grateful to A. E. Newhall for facilitating access to the data and to M. S. Ballard, J. Bonnel, M. G. Brown, N. R. Chapman, and S. E. Dosso for the benefit of our discussions. This work was supported by the National Science Foundation Grant No. OCE1657430, Binational Science Foundation Grant No. 2016545, and the Office of Naval Research Award Nos. N00014-18-WX01725 and N00014-19-WX00462.

https://doi.org/10.1121/10.0001333

References and links

[1]P. Roux, W. A. Kuperman, and NPAL Group, "Extracting coherent wave fronts from acoustic ambient noise in the ocean," J. Acoust. Soc. Am. **116**, 1995–2003 (2004).

[2]K. G. Sabra, P. Roux, A. M. Thode, G. L. D'Spain, W. S. Hodgkiss, and W. A. Kuperman, "Using ocean ambient noise for array self-localization and self-synchronization," IEEE J. Oceanic. Eng. **30**, 338–347 (2005).

[3]O. A. Godin, "Recovering the acoustic Green's function from ambient noise cross-correlation in an inhomogeneous moving medium," Phys. Rev. Lett. **97**, 054301 (2006).

[4]O. A. Godin, N. A. Zabotin, and V. V. Goncharov, "Ocean tomography with acoustic daylight," Geophys. Res. Lett. **37**(13), L13605, https://doi.org/10.1029/2010GL043623 (2010).

[5]O. A. Godin, M. G. Brown, N. A. Zabotin, L. Zabotina, and N. J. Williams, "Passive acoustic measurement of flow velocity in the Straits of Florida," Geosci. Lett. **1**, 16 (2014).

[6]K. F. Woolfe, S. Lani, K. G. Sabra, and W. A. Kuperman, "Monitoring deep-ocean temperatures using acoustic ambient noise," Geophys. Res. Lett. **42**, 2878–2884, https://doi.org/10.1002/2015GL063438 (2015).

[7]L. G. Evers, K. Wapenaar, K. D. Heaney, and M. Snellen, "Deep ocean sound speed characteristics passively derived from the ambient acoustic noise field," Geophys. J. Int. **210**, 27–33 (2017).

[8]F. Li, X. Yang, Y. Zhang, W. Luo, and W. Gan, "Passive ocean acoustic tomography in shallow water," J. Acoust. Soc. Am. **145**(5), 2823–2830 (2019).

[9]E. K. Skarsoulis and B. D. Cornuelle, "Cross-correlation of shipping noise: Refraction and receiver-motion effects," J. Acoust. Soc. Am. **145**(5), 3003–3010 (2019).

[10]K. G. Sabra, P. Roux, and W. A. Kuperman, "Emergence rate of the time-domain Greens function from the ambient noise cross-correlation function," J. Acoust. Soc. Am. **118**, 3524–3531 (2005).

[11]O. A. Godin, "Acoustic noise interferometry in a time-dependent coastal ocean," J. Acoust. Soc. Am. **143**(2), 595–604 (2018).

[12]A. E. Newhall, T. F. Duda, K. von der Heydt, J. D. Irish, J. N. Kemp, S. A. Lerner, S. P. Liberatore, Y. T. Lin, J. F. Lynch, A. R. Maffei, A. K. Morozov, A. Shmelev, C. J. Sellers, and W. E. Witzell, "Acoustic and oceanographic observations and configuration information for the WHOI moorings from the SW06 experiment," No. WHOI-2007-04, Woods Hole Oceanographic Institution, Woods Hole, MA (2007).

[13]D. Tang, J. Moum, J. Lynch, P. Abbot, R. Chapman, P. Dahl, T. Duda, G. Gawarkiewicz, S. Glenn, J. Goff, H. Graber, J. Kemp, A. Maffei, J. Nash, and A. Newhall, "Shallow Water '06: A joint acoustic propagation/Nonlinear internal wave physics experiment," Oceanogr. **20**(4), 156–167 (2007).

[14]J. Bonnel and N. R. Chapman, "Geoacoustic inversion in a dispersive waveguide using warping operators," J. Acoust. Soc. Am. **130**(2), EL101–EL107 (2011).

[15]J. Bonnel, S. E. Dosso, D. Eleftherakis, and N. R. Chapman, "Trans-dimensional inversion of modal dispersion data on the New England Mud Patch," IEEE J. Ocean. Eng. **45**(1), 116–130 (2020).

[16]T. W. Tan, O. A. Godin, M. G. Brown, and N. A. Zabotin, "Characterizing the seabed in the Straits of Florida by using acoustic noise interferometry and time warping," J. Acoust. Soc. Am. **146**(4), 2321–2324 (2019).

[17]M. G. Brown, "Time-warping in underwater acoustic waveguides," J. Acoust. Soc. Am. **147**(2), 898–910 (2020).

[18]See supplementary material at http://dx.doi.org/10.1121/10.0001333 for a discussion of the effect of variations of the sound speed in the water column on normal mode travel times and a detailed comparison of results of the passive and active geoacoustic inversions at the SW06 site.

[19]J.-X. Qin, B. Katsnelson, O. Godin, and Z.-L. Li, "Geoacoustic inversion using time reversal of ocean noise," Chin. Phys. Lett. **34**(9), 094301 (2017).

[20]F. Auger and P. Flandrin, "Improving the readability of time-frequency and time-scale representations by the reassignment method," Trans. Signal Process. **43**(5), 1068–1089 (1995).

[21]O. A. Godin, B. Katsnelson, and T. W. Tan, "Normal mode dispersion and time warping in the coastal ocean," J. Acoust. Soc. Am. **146**(3), EL205–EL211 (2019).

[22]M. B. Porter, "The KRAKEN Normal Mode Program," La Spezia, Italy (SACLANT Undersea Research Centre SM-245, 1991).

[23]P. Gerstoft, "Inversion of seismoacoustic data using genetic algorithms and a posteriori probability distribution," J. Acoust. Soc. Am. **95**(2), 770–782 (1994).

[24]Y. M. Jiang, N. R. Chapman, and P. Gerstoft, "Estimation of geoacoustic properties of marine sediment using a hybrid differential evolution inversion method," IEEE J. Oceanic Eng. **35**(1), 59–69 (2010).

[25]G. V. Frisk, K. M. Becker, S. D. Rajan, C. J. Sellers, K. Von Der Heydt, C. M. Smith, and M. S. Ballard, "Modal mapping experiment and geoacoustic inversion using sonobuoys," IEEE J. Oceanic Eng. **40**(3), 607–620 (2014).

[26]L. Wan, M. Badiey, and D. P. Knobles, "Geoacoustic inversion using low frequency broadband acoustic measurements from L-shaped arrays in the Shallow Water 2006 Experiment," J. Acoust. Soc. Am. **140**(4), 2358–2373 (2016).

[27]L. A. Brooks and P. Gerstoft, "Green's function approximation from cross-correlations of 20-100 Hz noise during a tropical storm," J. Acoust. Soc. Am. **125**(2), 723–734 (2009).

[28]L. A. Brooks, P. Gerstoft, and D. P. Knobles, "Multichannel array diagnosis using noise cross-correlation," J. Acoust. Soc. Am. **124**(4), EL203–EL209 (2008).

[29]T. Tan, O. A. Godin, A. Lefebvre, W. Beaute, B. G. Katsnelson, and M. Yarina, "Characterizing the seabed by using noise interferometry and time warping," Proc. Mtgs. Acoust. **35**, 070001 (2018).

[30]J. Bonnel, S. P. Pecknold, P. C. Hines, and N. R. Chapman, "An experimental benchmark for geoacoustic inversion methods," IEEE J. Oceanic Eng. **45**, 1–22 (2020).